Journal of Physical Science and Environmental Studies
Vol. 2 (1), pp. 6-22, April, 2016
ISSN 2467-8775
Full Length Research Paper
http://pearlresearchjournals.org/journals/jpses/index.html

On the Rough Sea Occurrence and its trend in the South China Sea

Osinowo Adekunle Ayodotun[1*], Xiaopei Lin[1], Zhao Dongliang[1] and Wang Zhifeng[2]

Accepted 21 March, 2016

[1]College of Physical and Environmental Oceanography, Ocean University of China, Qingdao, 266100 , China.
[2]College of Engineering, Ocean University of China, Qingdao, 266100, China.

ABSTRACT

This paper presents a thirty year (1976 to 2005) spatio-temporal variation and trends in the occurrence of rough sea events in the South China Sea (SCS). The largest percentage frequencies of rough sea occurred around large regions within the central and northern SCS. Rough sea occurrence is highest during winter (up to 16%). In the central SCS, rough sea occurred most often (25 to 30%) in December. The regional distribution of the annual trends of rough sea occurrence showed that increasing trends are most significant (0.1%-0.13% yr^{-1}) around Luzon strait and adjacent waters. The area extent of the significant increase in rough sea is largest in winter. A significant increasing trend in rough sea occupied the largest region in the northern and central SCS in December with the strongest trend (up to 1% yr^{-1}) around Xisha. The rough sea exhibits a significant increasing trend of 0.032%yr^{-1} as a whole in the SCS. The trend (0.12%yr^{-1}) is strongest in winter. Monthly and diurnal trend analysis also showed that the trend is most significant in December (0.25% yr^{-1}) and at 0hr (0.034% yr^{-1}). Areas around Hainan, Kalimantan and Palawan with general low values of rough sea occurrence are associated with shadowing, island blocking, refraction or complex topography.

Key words: Annual, Percentage, Seasonal, Significant, Monthly, Significant wave height, Diurnal and Wave watch III (WW3)

*Corresponding author E-mail:voxfox99@yahoo.com.

INTRODUCTION

The South China Sea (SCS) is the deepest and largest sea around China with an average water depth of 1212 m and a maximum depth of 5567 m. It is a marginal sea that is part of the Pacific Ocean, encompassing an area from the Singapore and Malacca Straits to the Strait of Taiwan of around 3,500,000 square kilometres (1,400,000 sq mi). The area's importance largely results from one-third of the world's shipping sailing through its waters and that it is believed to hold huge oil and gas reserves beneath its seabed. After the Coral Sea and Arabian Sea, it is the third largest epi-continental sea in the global oceans. The SCS is a half-enclosed tropical sea within complex topography between the Asian landmass to the north and west, the Philippine Islands to the east, Borneo to the southeast, and Indonesia to the south Chu and Cheng (2008). The water volume is 3.5 to 3.85 million cubic square meters, which is about 13 times that of the total volume of the East China Sea, the Yellow Sea, and the Bohai Sea. The SCS is under the influence of monsoon winds and synoptic systems such as fronts and tropical cyclones (Chu et al., 1999a; Edmons and Fan, 1999b; Veneziano and Fan, 2000).

Turbulence associated with sea waves promotes interchange between the sea and atmosphere, as well as circulation and distribution of oxygen, heat and other elements within the upper layer of the ocean Moon, (2005).

Ocean wave has a huge impact on human lives and activities. Studies have shown that casualties caused by wave disasters are in the first place of all maritime

disasters Zheng et al., (2013a) especially the surge, it is often with amazing destructive power, which makes the ship hogging, sagging, propeller idling speed loss, buried shock, ran-out, bottomed aground, and other phenomenon, which will cause serious damage to the ship, even destroy it. Hogging is the stress a ship's hull or keel experiences that causes the center or the keel to bend upward. Sagging is the stress a ship's hull or keel is placed under when a wave is the same length as the ship and the ship is in the trough of two waves. This causes the middle of the ship to bend down slightly, and depending of the level of bend, may cause the hull to snap or crack. The rough sea can usually bring great impact on human lives.

Knowledge of wave characteristics is essential for the planning, design and construction of new ports coastal protection constructions, harbors and navigational channels (Schneggenburger et al., 2000; Sundar and Ananth, 1988) and it also contributes to fisheries activities, navigation, marine habitat management and coastal development and planning.

Ahmed, (2010) stated that with increasing frequency of occurrence of 'rough sea events', in the Bangladesh sea, the coastal fishermen are forced to stay out of action in anticipation of complete loss of investment made for fishing trips or forced to abandon incomplete fishing trips - the latter causing heavy financial losses. As a consequence of too many incomplete fishing trips and scanty return from subsequent investments, livelihoods of coastal fishermen have been devastated.

China is a big energy consuming country, the full development and utilization of marine energy will be beneficial to ease the global energy crisis. Knowledge of the rough sea occurrences and its changing trends are essential in the development of wave energy resource and can as well serve as references in navigation, marine engineering, disaster prevention and reduction in coastal environment. Until recently few studies have been carried out on the rough sea occurrences and its evaluation in the China seas. Zheng et al. (2014) made an investigation on the rough sea occurrence in the China Seas using a 10 year hindcast significant wave height data obtained from wave watch III (WW3) numerical wave model forced with QuikSCAT/NCEP (QN) wind data. They concluded that the occurrence is relative low, of below 14% in each season. The occurrence is highest in the winter, followed by the autumn and lowest in the spring. In this study, we extend the work by Zheng et al. (2014) in order to analyze the long-term spatio-temporal distribution of the timely trends in the percentage frequency of the rough sea. The paper is organized as follows. Section 2 provides information on the wave model setup and a thorough validation with altimeter data using some statistical tests with their results. Section 3 presents an analysis on the spatio-temporal variability and linear trends in the percentage frequency of the rough sea that is, SWH greater than 4.0 m as defined by Zheng et al. (2014) on an annual, seasonal, monthly and diurnal basis. Finally, conclusions of this study are given in section 4.

MODELS, DATA SETS AND METHODOLOGY

The Wave Model and Input Data

The model used for wave simulation is version 3.14 of the third-generation spectral wave model WAVEWATCH III ™ (denoted as WW3), Tolman (2009). WW3 was developed at the Ocean Modeling Branch of the Environmental Modeling Center of the National Centers for Environmental Prediction (NCEP) for the regional sea wave prediction. It was built on the base of Wavewatch-I and Wavewatch-II as developed at the Delft University of Technology, and NASA Goddard Space Flight Center, respectively Tolman, (2009). By using the NGDC (National Geophysical Data Center) ETOPO 1 data, with a resolution of 0.5 ° × 0.5 °, the SCS water depth field was processed by the Gridgen 3.0 packet. Source terms for energy spectra in the model are set to default. The model integrates the spectrum to a cut-off frequency, and above this frequency a parametric tail is applied. The boundary condition is cyclical. The other option settings are 36 directions, and 24 discrete wave-numbers (0.0412 ~ 0.4060Hz, 2.4 ~ 24.7s).

The model spatial grid covers the whole of SCS and part of ECS from longitudes 95^0E to 135^0E and latitudes 5^0S to 30^0N with a 0.25^0 resolution. The model in an operational/forecasting mode, was forced with 6 h re-analysis wind fields extracted over longitudes 95^0E to 135^0E and latitudes 5^0S to 30^0N from the weather research forecasting (WRF) model from 1976 to 2005 on a 0.2^0 (longitude) by 0.2^0 (latitude) Gaussian grid. Wind fields were interpolated on a regular 0.25^0 grid to force the model. The model output is a two-dimensional (2D) wave energy spectra obtained at each grid point with time period spanning from 1 January, 1976 to 31 December 2005 and with a 6 h output data. The model provides output of wave parameters including wave spectra, significant wave heights ($4\sqrt{}$ E), mean wavelength ($2\Pi k^{-1}$), mean wave period ($2\Pi k^{-1}2\pi$), mean wave direction, peak frequency, and peak direction. The simulation provided a 6 h time series of SWH and other wave parameters over a box extending from 3^0N to 23^0N and 105^0E to 121^0E which contains main part of SCS and surrounding waters. The available satellite data used in this study served as independent observations against which the modeled values were evaluated so no assimilation procedure was employed.

Satellite Data and Model Verification

Usually, the in-situ wind wave data are mainly collected

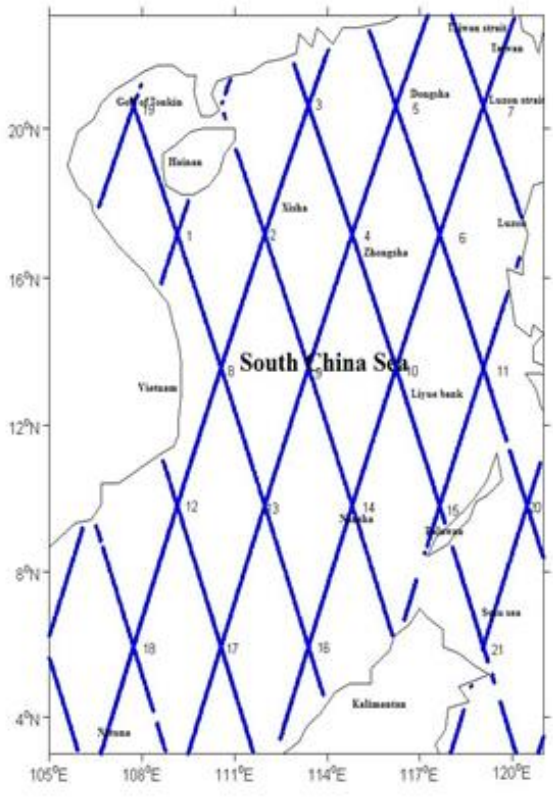

Figure 1. Topex/Poseidon crossover points and Geography of the SCS.

from voluntary ships and wave buoys. However, in SCS, sparse voluntary ship data and no wave buoy data are available. This makes the remote sensing (use of satellite data) be an important source for the wind wave data in the SCS.

The observation data used in this study were obtained from Topex/Poseidon (NASA/CNES) which is an official remote sensing data center that has data containing a near-real time grided observations for significant wave height. The Topex/Poseidon satellite, jointly launched by NASA and the French Space Agency, the Center National d'Etudes Spatiales (CNES) in August 1992, carried a state-of-the-art radar altimetry system Fu et al. (1994). In addition to precise measurements of the distance between the satellite and the surface, SWH was derived from the shape of the leading edge of the returning radar pulse. The accuracy of SWH measurement by Topex/Poseidon was within the accuracy of the Geosat measurements Callahan et al. (1994), that is, 10% or 0.5 m, whichever is greater Dobson et al. (1987). Topex/Poseidon was maneuvered into a 9.9156-day repeat period during which two Topex/Poseidon SWH data are available at each crossover point.

The TOPEX/Poseidon data was used to verify the accuracy of the WW3 simulations. The TOPEX/Poseidon satellite crossover points in the SCS in 2002 are shown in Figure 1. The model SWH data were interpolated into all the crossover points where the hindcast and altimeter data were computed. Comparisons were conducted between the model hindcast results and the Topex/Poseidon altimeter observations. The time series of the SWH between observations and simulations is shown in Figure 2a. The time series cover different periods in, 2002 for all the crossover points as Topex/Poseidon passed over the SCS.

Statistical Approaches-Methodology

Both observations and wave modeled data are studied by two statistical points of view: The first is based on descriptive statistical analysis methods where conventional indices are employed in order to capture the basic aspects of the data evolution spatially and temporally. The second approach is based on the study of the probability and cumulative density function that fits to the available data. This is a complementary approach being able to provide additional information for the shape and scale of the data in the study. In this way, a complete view of the main characteristics of observational and simulated significant wave height values is obtained.

Conventional Statistical Analysis

The skill of the model was evaluated through a statistical study that consists on calculating the following:

$$cc = \frac{\sum_{i-1}^{n}(x_i - \bar{x})(y_i - \bar{y})}{\sqrt{\sum_{i-1}^{n}(x_i - \bar{x})^2 \sum_{i-1}^{n}(y_i - \bar{y})^2}} \quad (1)$$

$$Bias = \bar{y} - \bar{x} \quad (2)$$

$$RMSE = \sqrt{\frac{1}{N}\sum_{i-1}^{n}(y_i - x_i)^2} \quad (3)$$

Where, xi represents the observed data, y_i represents the simulated data, x and y are mean value of observed and simulated data, N is the total number of observations. Figure 2b shows the scatter diagrams around the line where the observed and simulated SWH are equal. The correlation coefficient (cc) between the simulated and observed data is 0.914. From Bias which is 0.012m, we find that the model slightly overestimates the observed SWH. The RMSE between the simulated and observed data is 0.432m indicating a low error of simulated data.

The distributions of Bias, RMSE and CC for the whole year (2002) are also shown (Figure 2c) to understand the spatial error variability. The Bias varies from -0.43 m at point 18 (107.7^{0}E, 20.59^{0}N) to 0.36 m at point 7 (114.8^{0}E, 9.81^{0}N). Positive Bias dominates the SCS. In the Gulf of Tonkin, Point 19 (107.7^{0}E, 20.59^{0}N), negative Bias is greater than -0.4 m and a positive Bias larger than 0.32 m is found very close to Nansha Island, point 14 (114.8^{0}E, 9.81^{0}N). The RMSE ranges between 0.28 m at point 18 (107.7^{0}E, 5.93^{0}N) and 0.94 m at point 4 (114.81^{0}E, 17.19^{0}N).

The RMSE of SWH is generally above 0.45 m in the central SCS and decreases southwards. The CC of SWH between modeled and Topex/Poseidon data in 2002 is larger than 0.8 almost everywhere in SCS except in the Gulf of Tonkin in which CC is less than 0.6. The CC range between 0.53 at point 19 (107.7^{0}E, 20.59^{0}N) and 0.96 at point 4 (114.81^{0}E, 17.19^{0}N). Presented in Figure 2d is the temporal error of the monthly mean Bias and RMSE averaged over all the crossover points in the SCS. The Bias varies from -0.0147 m in April to 0.051 m in March which shows that WW3 has a very low bias in predicting the SWH. The RMSE has a minimum value (0.33 m) in April and a maximum value (0.496 m) in December.

Probability and Cumulative Density Functions

The monthly mean data obtained for the significant wave height in the SCS, as interpolated and simulated at all cross over points are studied here focusing on distributions that they form. In this study, two-parameter Weibull distribution function (WDF) is employed to describe the monthly SWH variation. The probability density function (PDF) for Weibull, can be expressed as:

$$f(v) = \frac{k}{c}\left(\frac{v}{c}\right)^{k-1} \exp\left[-\left(\frac{v}{c}\right)^{k}\right] \quad (4)$$

While the corresponding cumulative density functions (CDF) is given as:

$$\mathrm{F}(v) = 1 - \exp\left[-\left(\frac{v}{c}\right)^{k}\right] \quad (5)$$

Where v is the monthly averaged SWH for all cross over points, while k and c are known as shape and scale parameters, respectively. The standard deviation method as expressed in Equations 6 and 7 is used to calculate these parameters.

$$k = -\left(\frac{\sigma}{\bar{v}}\right)^{-1.086} \quad (6)$$

$$c = \frac{\bar{v}}{\Gamma\left(1+1/k\right)} \quad (7)$$

v is the monthly mean SWH, σ is the standard deviation which shows degree of variation of SWH and Γ(x) is the gamma function which is given by:

$$\Gamma\left(x\right) = \int_0^{\infty} \exp\left(-u\right) u^{x-1} dx \quad (8)$$

The Weibull PDF and CDF plots are presented in Figures 2e for satellite records and their WW3 counterparts. Same plots have been made in Figures 2f but for the Weibull scale and shape parameters. The plots have nearly identical patterns. The PDF for the observed SWH ranged between 0.53 and 2.33 while for simulations, it ranged between 0.52 and 0.61. Also for the CDF, the observed SWH ranged between 0.52 and 0.6 and for simulations, CDF varies between 0.53 and 0.61. The Weibull scale parameter varies between 0.45 and 1.66 for observations and between 0.55 and 1.65 for simulations. Also for the Weibull shape parameter, the observed SWH ranged between 1.23 and 2.67 and for simulations, CDF varies between 1.14 and 2.31. In general, the simulation results are consistent with the observations, which indicate that in general the WW3 can well reproduce the SWH and as well be a dependable model to simulate surface waves in the SCS.

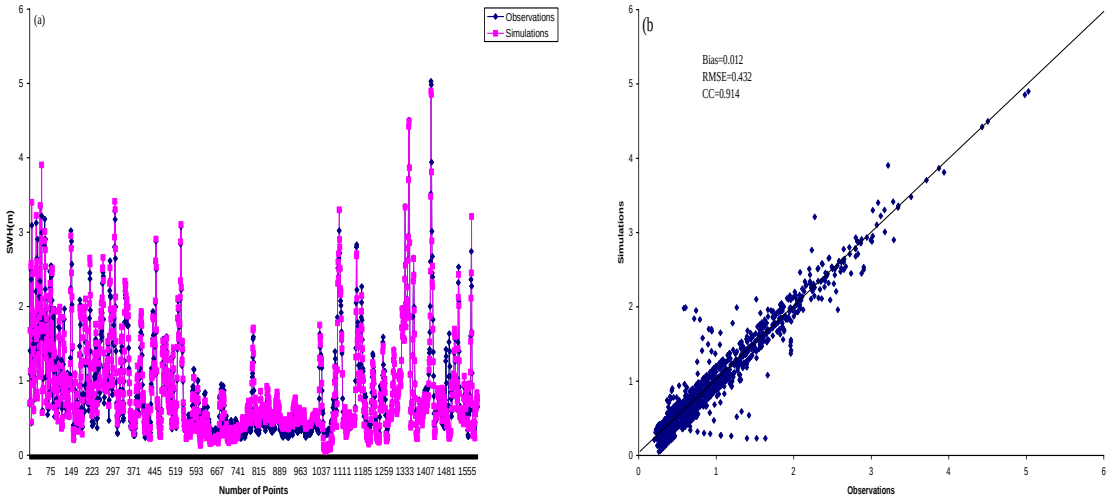

Figure 2. (a) Time series of the wave model data against Topex/Poseidon data for the SWH, on the x-axis is the number of data points. (b) Scatter plot of the wave model data against Topex/Poseidon data for the SWH. From 01 January 2002 to 31 December 2002.

Wave climate of the SCS

The SCS is influenced by monsoon winds and synoptic systems such as fronts and tropical cyclones. The winter monsoon season is from October to March, in which northeast wind prevails and cold fronts influence the SCS; the summer monsoon season is from June to August, with anticyclones and enhanced convection migrating northward from the equator to the mid-latitudes. The sea-surface wind over the SCS is strongest during the winter monsoon and weaker during the summer monsoon. In the periods of seasonal transition, spring and autumn, the average wind speed is smaller than in summer and winter. The tropical cyclone (TC) is a very important weather factor that influences the SCS in summer and autumn. The central and northern parts of the SCS (19°– 20°N, 110°–120°E) are core regions where the TC forms. In the SCS, the propagating direction of the TC is mainly west-forward and more than 25 TCs occur every year, mostly from July to October Wang et al., (2014). The combination of storm frequency, duration, and intensity, and the geographic characteristics of the ocean basins, determine the properties of the SCS wave field and its seasonal variation.

Spatio-Temporal Variability and Linear Trends in Rough Sea Occurrence

Spatial Distribution of the Rough Sea Occurrence

The rough sea occurrence (%) climatology for the SCS has been determined by means of the SWH hindcast data. By calculating the regional average percentage frequency of rough sea (SWH>4 m) from 00:00 UTC on January 1, 1976, to 18:00 UTC on December 31, 1976, spatial yearly average values were obtained. Same computation was carried out for subsequent years and we obtained 30 yearly average values of the rough sea occurrence in the SCS to analyze the overall annual mean distribution for 1976 to 2005, as shown in Figure 3. The same method was also done to obtain the overall seasonal, monthly and diurnal mean distribution for the 30 year period, as shown respectively in Figures 4, 5 and 6. As regards the annual average distribution characteristics, the areas with largest values are located around Xisha, Zhongsha, Dongsha and

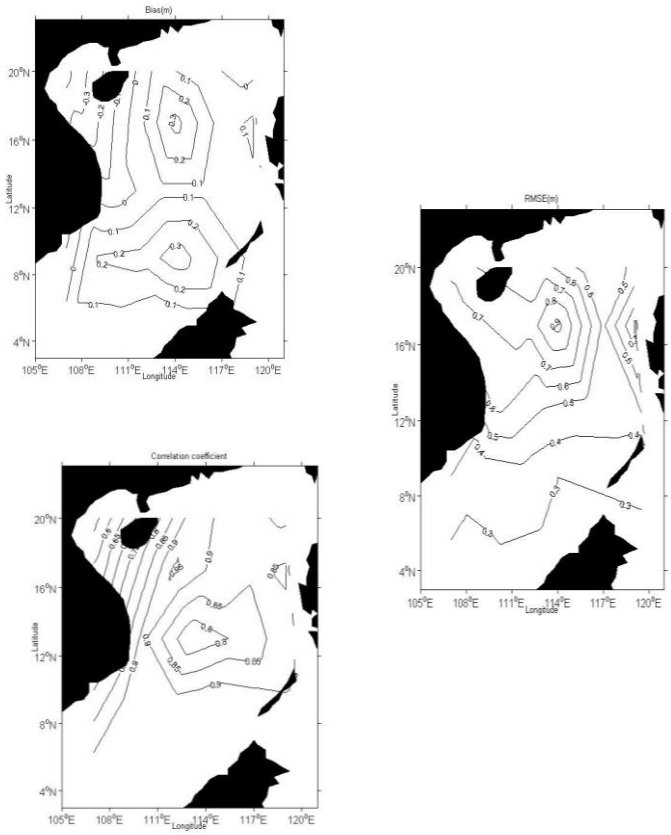

Figure 2c. Distributions of SWH: Bias, RMSE error and correlation coefficient between WW3 and Topex/Poseidon data.

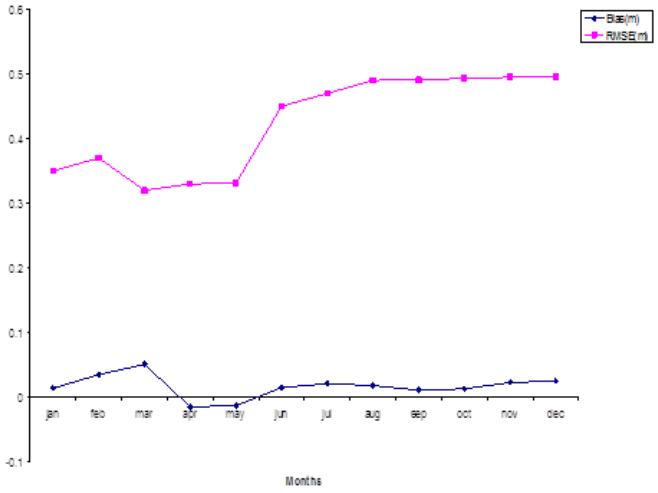

Figure 2d. Temporal error variability of the Bias and RMSE between WW3 and Topex/Poseidon data for all the crossover points.

Luzon strait. The rough sea occurrence is below 2% in regions around Hainan, Taiwan and in many waters below latitude 12oN including Kalimantan and Palawan. Most regions immediate North and South of the central SCS have rough sea occurrence between 2 and 7%. In all, the rough sea occurrence is between 2 and 9% in virtually all parts of the SCS.

The rough sea occurrence in the SCS is below 17% in each season as shown in Figure 4. In the winter, the rough sea occurrence is obviously greater than those of the other seasons due to the predominance of the Northeast trade wind caused by frequent and powerful

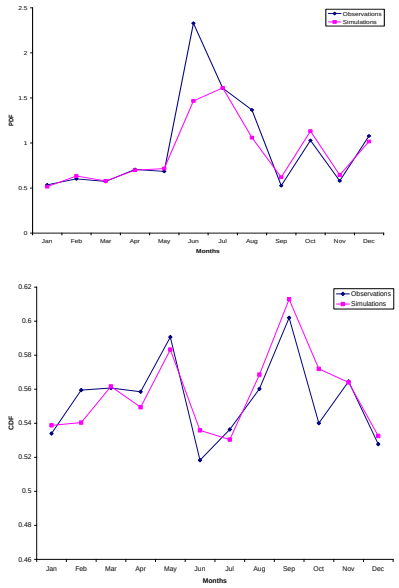

Figure 2e. The evolution of PDF and CDF for monthly mean value of WW3 simulated and satellite recorded significant wave height for all cross over points in 2002.

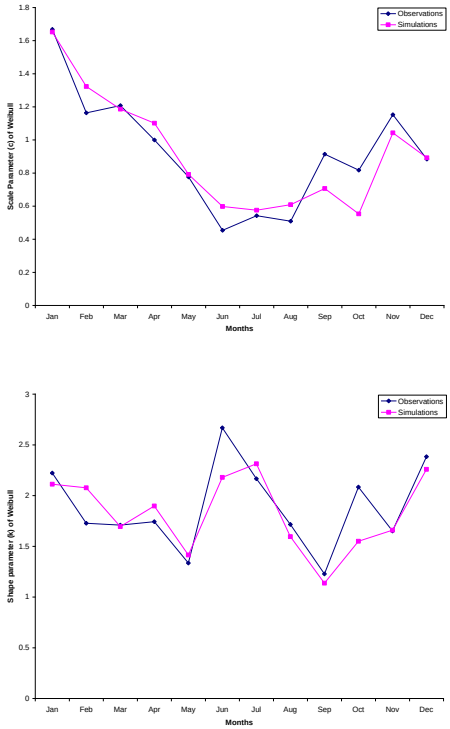

Figure 2f. The evolution of Weibull scale and shape parameters for monthly mean value of WW3 simulated and satellite recorded significant wave height for all cross over points in 2002.

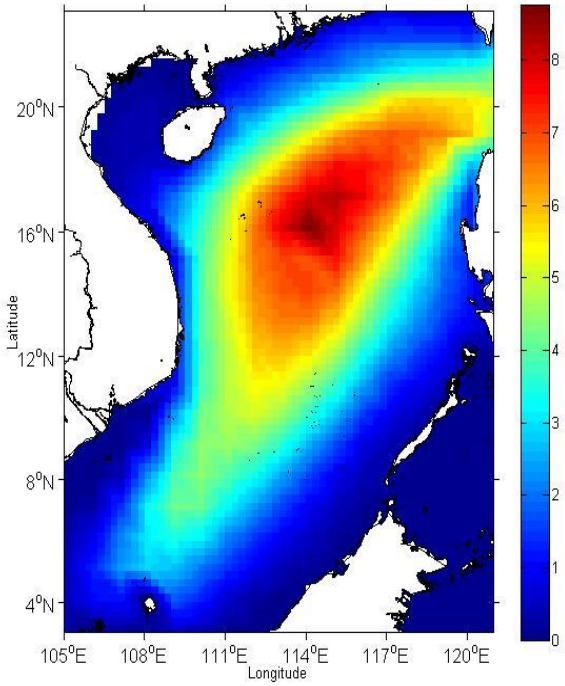

Figure 3. Annual mean rough sea occurrence percentage in the SCS based on the wave hindcast information (1976 to 2005).

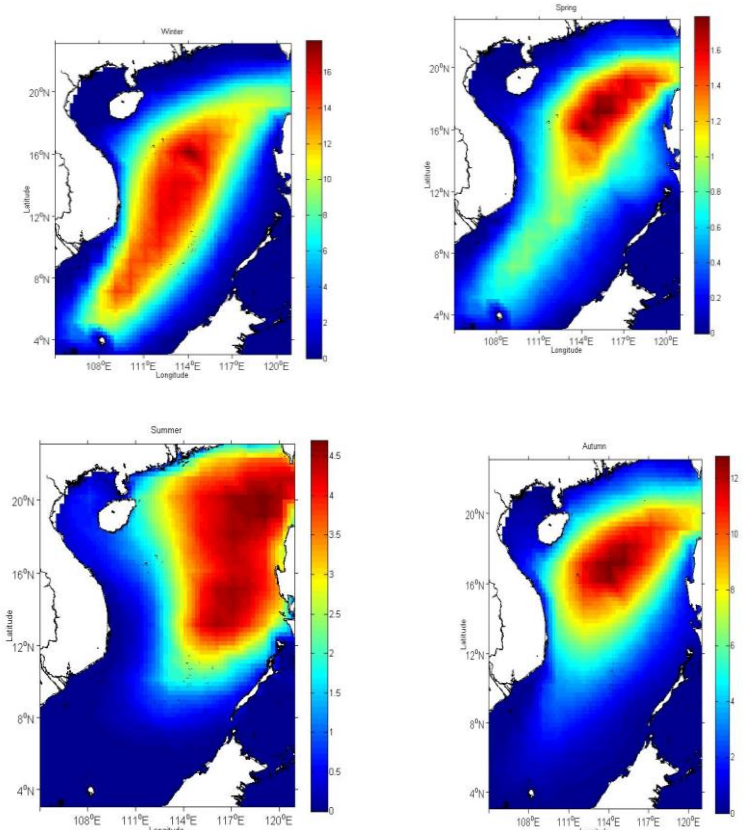

Figure 4. Seasonal mean rough sea occurrence percentage in the SCS based on the wave hindcast information (1976 to 2005).

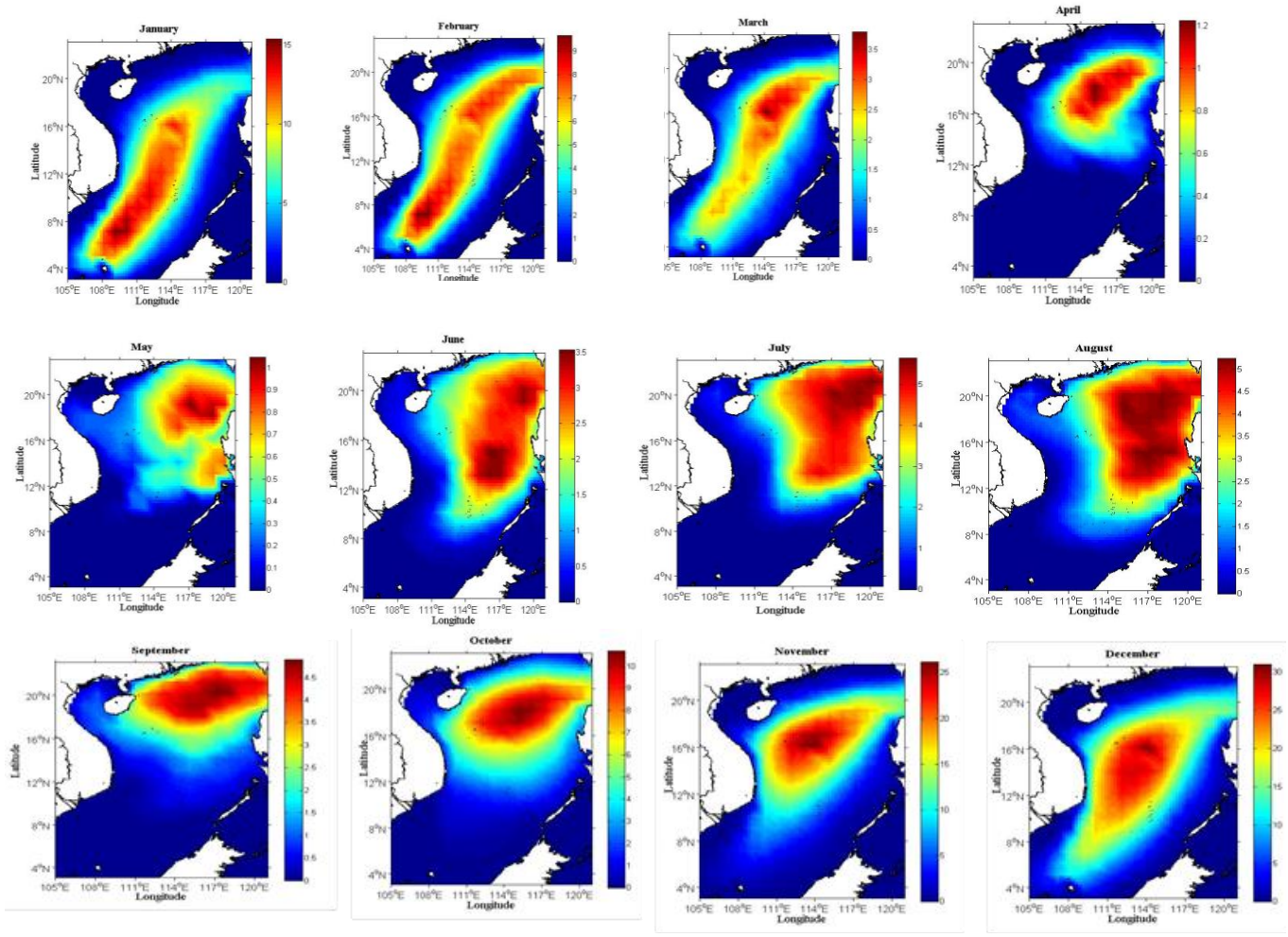

Figure 5. Monthly mean rough sea occurrence percentage in the SCS based on the wave hindcast information (1976 to 2005).

cold air. Largest values (10 to 16%) centre around Xisha, Zhongsha, Dongsha and Luzon strait. Least values (<3%) are noted Northwest and Northeast of Hainan, waters onthe borders of Vietnam and in some regions around Kalimantan and Palawan in the Southern SCS. The rough sea occurrence in the spring is least in the whole years (<1.6%) in most part of the SCS. Largest values (1 to 1.6%) distribute around Xisha, Zhongsha, Dongsha and Luzon strait.

The rough sea occurrence is least (<0.4%) in waters around Hainan, Taiwan, Kalimantan, Palawan and around the borders of Vietnam. During summer, the rough sea occurrence is a bit higher than in spring, but less than 5% in most of the SCS. Largest values (2.5 to 4.8%) are seen around the central SCS, Zhongsha and waters adjacent Luzon. Values below 1% are found Northwest of Hainan, around Vietnam borders and in most waters of the Southern SCS.

The rough sea occurrence in autumn is clearly greater than in spring and summer but less than 14% in most waters of SCS. Large area of rough sea occurrence distribute around Xisha, Zhongsha, Dongsha and Luzon strait approximately (8 to 12%). Locations around Hainan, Vietnam borders and most waters in the Southern SCS have values below 2%. These are very close to the findings of Zheng et al. (2014). In Figure 5, the percentage frequency of rough sea is largest in November through January. A high percentage of rough seas occur over a large part of the SCS in November, December and January. Peak values (25 to 30%) are centered around Xisha, Zhongsha, Dongsha and Luzon strait in December. Largest values (10 to 15%) are seen in some regions in the central and southern SCS in January. In November, the largest values (15 to 25%) concentrate over a large portion of the northern SCS, particularly around Luzon strait and its adjacent waters. The percentage frequency of rough sea is relatively large in October and February. Largest occurrences (8 to 10%) for both months are found around Xisha, Zhongsha and Luzon strait. High values (8- to 10%) also centre around

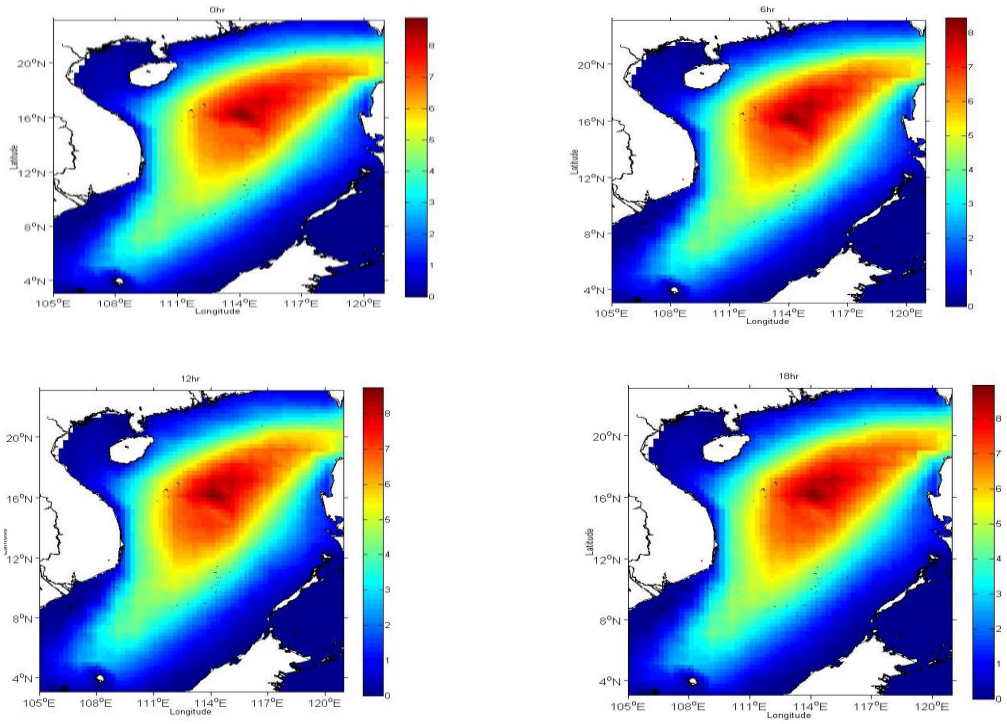

Figure 6. Diurnal mean rough sea occurrence percentage in the SCS based on the wave hindcast information (1976 to 2005).

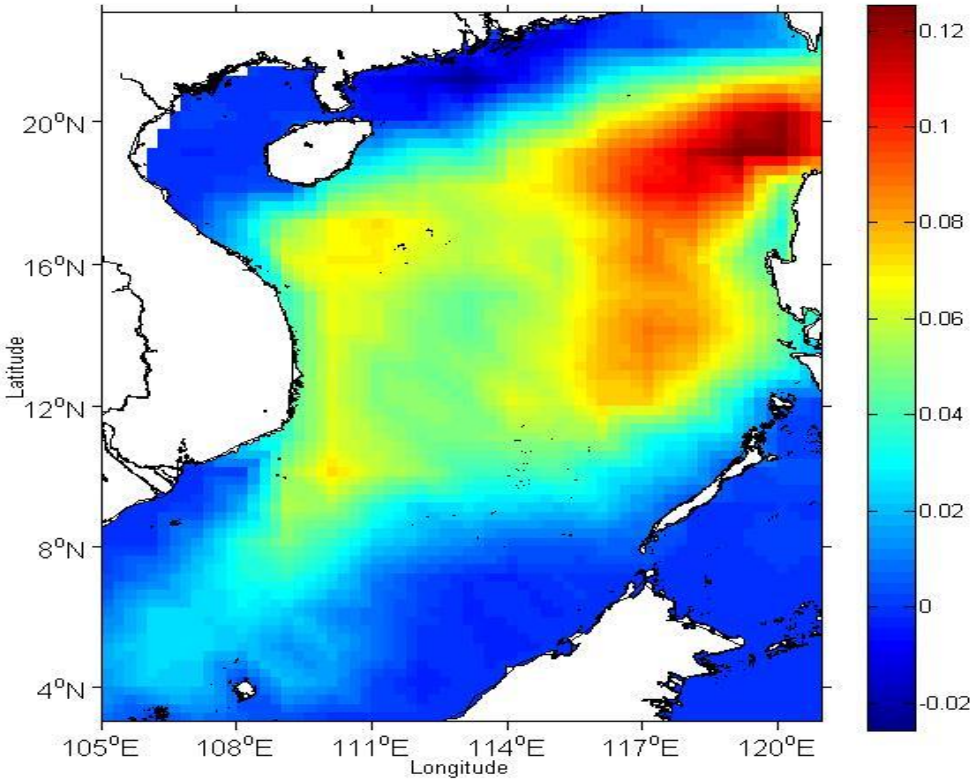

Figure 7. Linear trends in annual rough sea occurrence (% yr^{-1}) in the SCS based on the wave hindcast information (1976 to 2005).

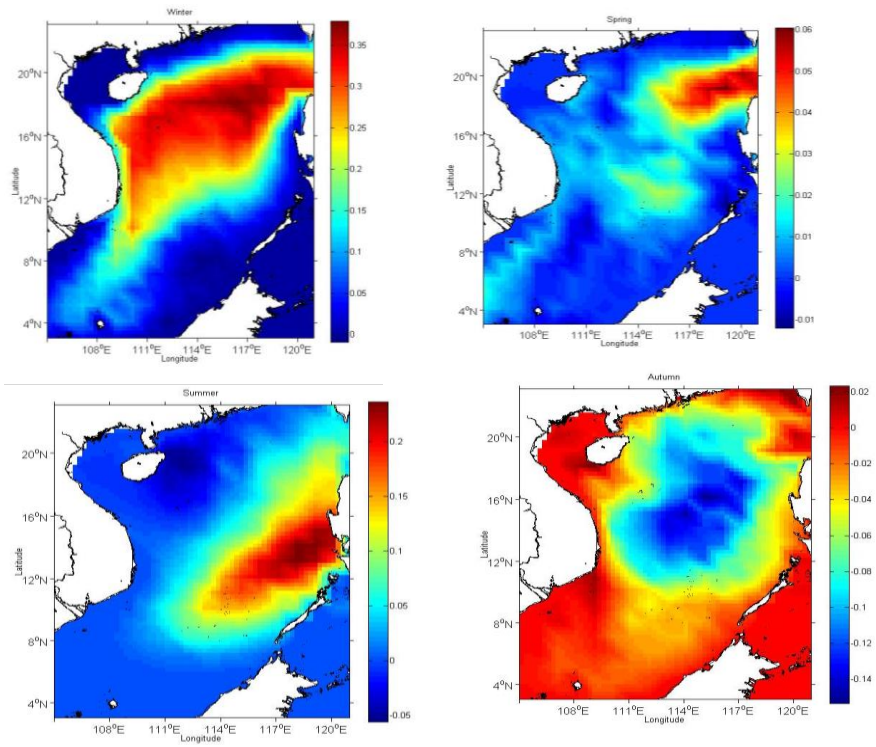

Figure 8. Linear trends in seasonal rough sea occurrence (% yr^{-1}) in the SCS based on the wave hindcast information (1976 to 2005).

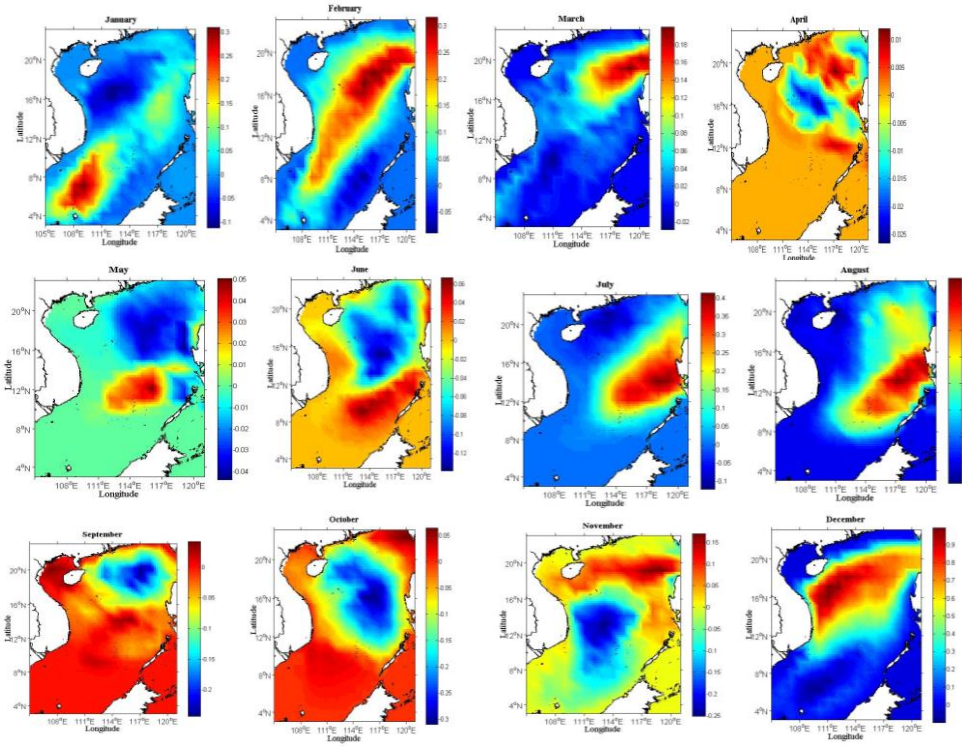

Figure 9. Linear trends in monthly rough sea occurrence (% yr^{-1}) in the SCS based on the wave hindcast information (1976 to 2005).

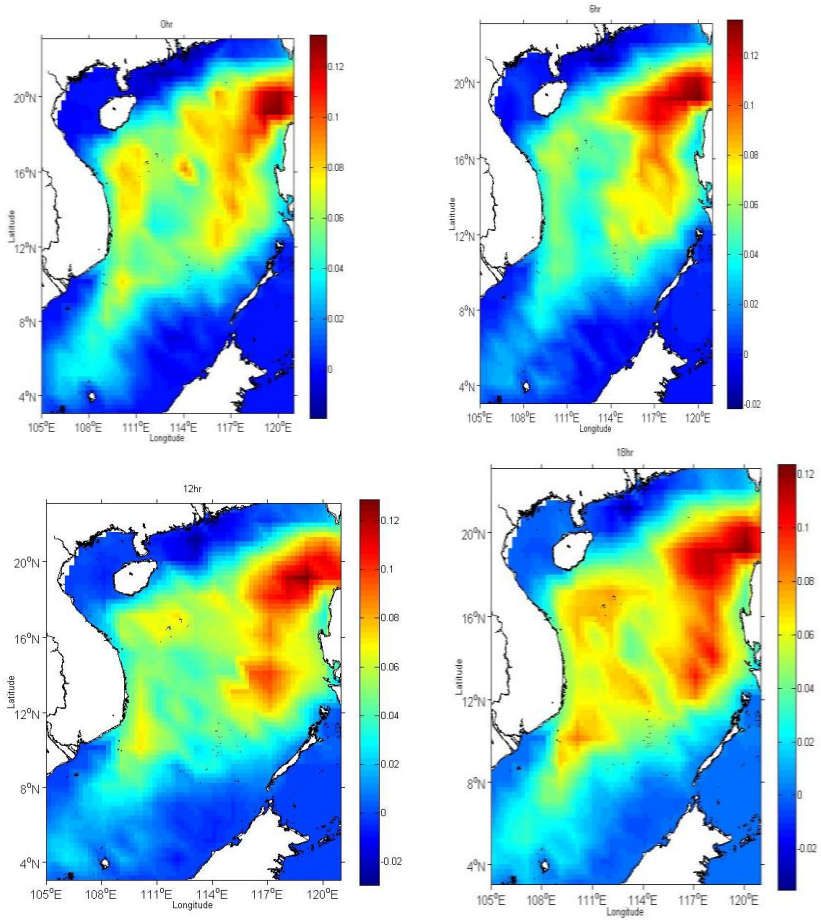

Figure 10. Linear trends in diurnal rough sea occurrence (% yr^{-1}) in the SCS based on the wave hindcast information (1976 to 2005).

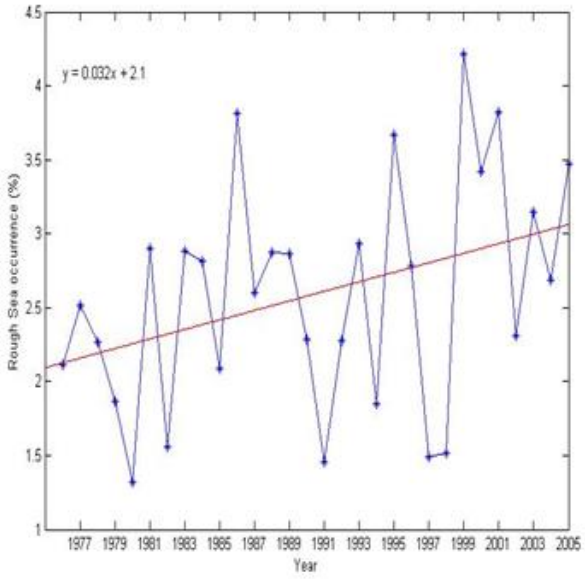

Figure 11. Linear trend and variation of the annual mean rough sea occurrence percentage in the SCS based on the wave hindcast information (1976 to 2005).

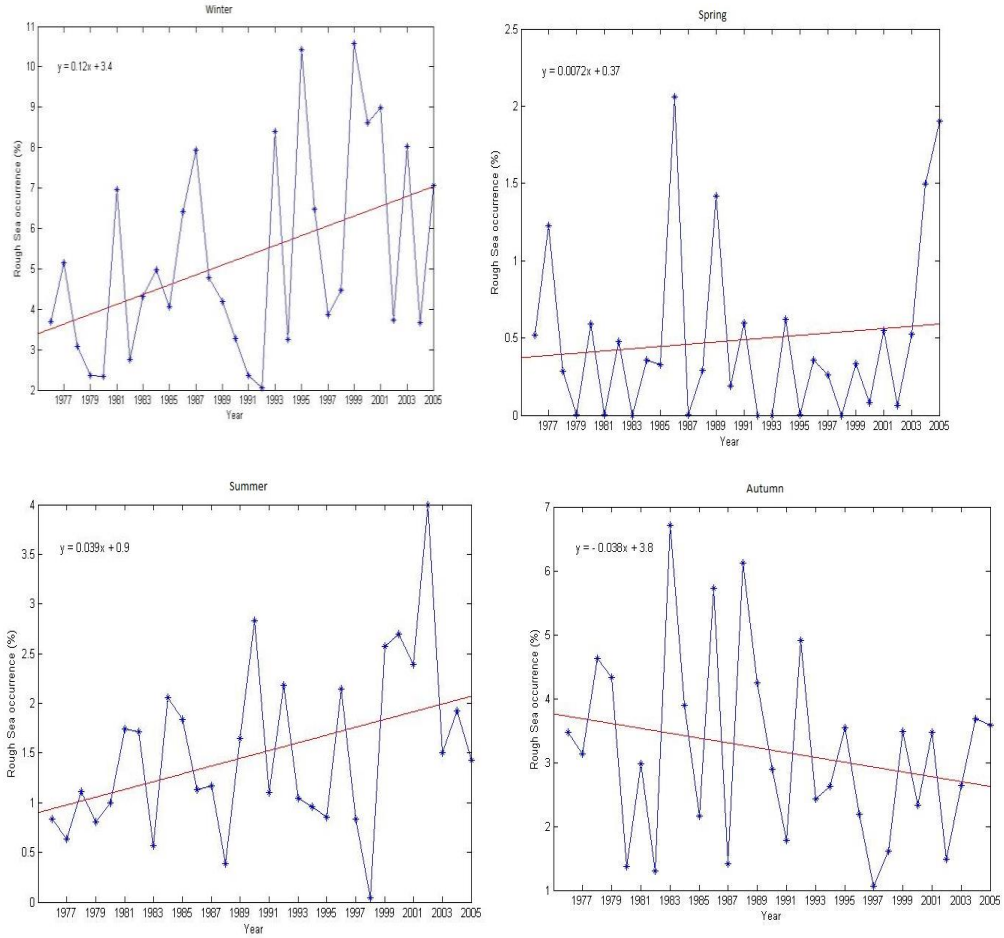

Figure 12. Linear trends and variations of the seasonal mean rough sea occurrence (% yr^{-1}) in the SCS based on the wave hindcast information (1976 to 2005).

a small portion of the southern SCS in February. From March through September, the percentage frequency of rough sea is largest over most part of the northern SCS particularly in regions close to Taiwan and around Luzon strait. High values are also noticed around Luzon from May through August. In nearly all months, low percentage frequency of rough sea dominates the southern SCS and in few regions in the northern SCS. In Figure 6, the rough sea occurrence does not show much diurnal variation in the SCS. For the hours (0hr,6.00hr,12.00hr and 18.00hr) considered, the percentage frequency of the rough sea is largest around Luzon strait, Dongsha, Xisha and Zhongsha which are in the northern and central SCS. The percentage frequency is smaller in other regions of the SCS.

Spatial Distribution of Long-Term Trends in Rough Sea Occurrence

The spatial distributions of the annual, seasonal, monthly and diurnal trends in the rough sea occurrence are as shown in Figures 7, 8, 9 and 10. From Figure 7, positive trends dominate most part of the SCS. The relative large region distribute in the central and northern area of SCS. Increasing trends are most significant (0.1 to 0.13% yr^{-1}) around Luzon strait and adjacent waters. Negative trends between 0 and -0.02% yr^{-1} are observed in few small regions in the northern and southern SCS. As shown in Figure 8, the long-term trend in the rough sea occurrence in the SCS showed great seasonal differences. The area extent of the significant increase in rough sea occurrence is largest in winter; the area decreased in summer and spring, with the smallest area in autumn. In winter, positive trends dominate all parts of the SCS. Areas with a relatively strong increase (0.3 to 0.37% $yr^{-1)}$ locate around Luzon strait, Zhongsha, Xisha and Dongsha. In spring, positive trends dominate most part of the SCS. Areas with most significant increase of between 0.04% yr^{-1} and 0.06% yr^{-1} are mainly distributed around Luzon strait and its adjacent waters. In summer, negative trends occupy large water bodies in the northern and southern SCS. The negative trend is strongest (-0.05% yr-1) to the east of Hainan island. Increasing positive

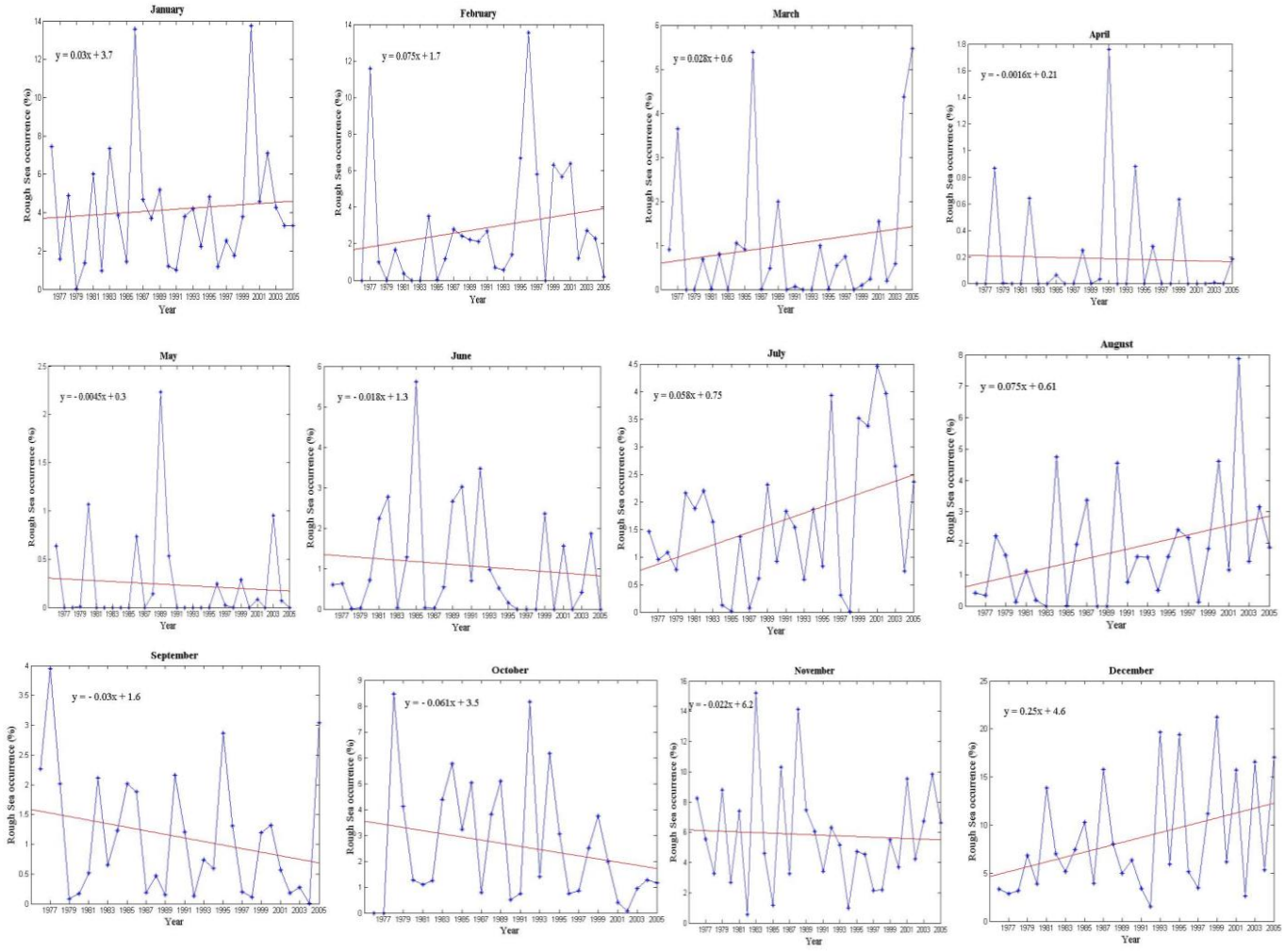

Figure 13. Linear trends and variations of the monthly mean rough sea occurrence (%yr^{-1}) in the SCS based on the wave hindcast information (1976 to 2005).

trends are noticed around Luzon strait and its adjacent waters down to waters surrounding Luzon where the trend is the strongest of approximately (0.25% yr^{-1}). In autumn, negative trends dominate most part of the central and northern SCS. Positive trends of 0.02% yr^{-1} are only noticed in small regions around Hainan Island and Taiwan. Negative trends are especially strongest around Xisha and Zhongsha of between -0.12% yr^{-1} and -0.14% yr^{-1}. During autumn, the trends are stronger in the southern SCS than in other regions. The increasing trend is generally strongest in winter, followed by summer and spring and weakest in autumn.

In Figure 9, the trends in the rough sea occurrence are nearly insignificant (0.05 to 0% yr^{-1}) in most regions of the SCS during July and August. Strong increasing trends (0.25 to 0.4% yr^{-1}) are seen around Luzon and its west waters in the central SCS. The rough sea occurrence exhibits significant increasing trends around Luzon strait, Dongsha and adjacent waters in the northern SCS during December, February, March and November. The trends are insignificant and decreasing over the rest regions. The trend in rough sea occurrence is strongest (up to 1% yr^{-1}) around Xisha in December. Significant increasing trends in rough sea occurrence exist in some waters in the southwest and central SCS respectively in January, June and May. Also in these months, the rough sea occurrence exhibits insignificant and negative trends in every part of the northern SCS. In May, negative trends dominate most part of the SCS. Insignificant and decreasing trends are seen in every part of the SCS in April, October and September. As shown in Figure 10, the trends in rough sea occurrence do not show much diurnal differences in the SCS. In all the hours considered, relatively large area of significant increasing trends (0.02 to 0.14% yr^{-1}) occurs in most waters of the central and northern SCS. The trends in rough sea

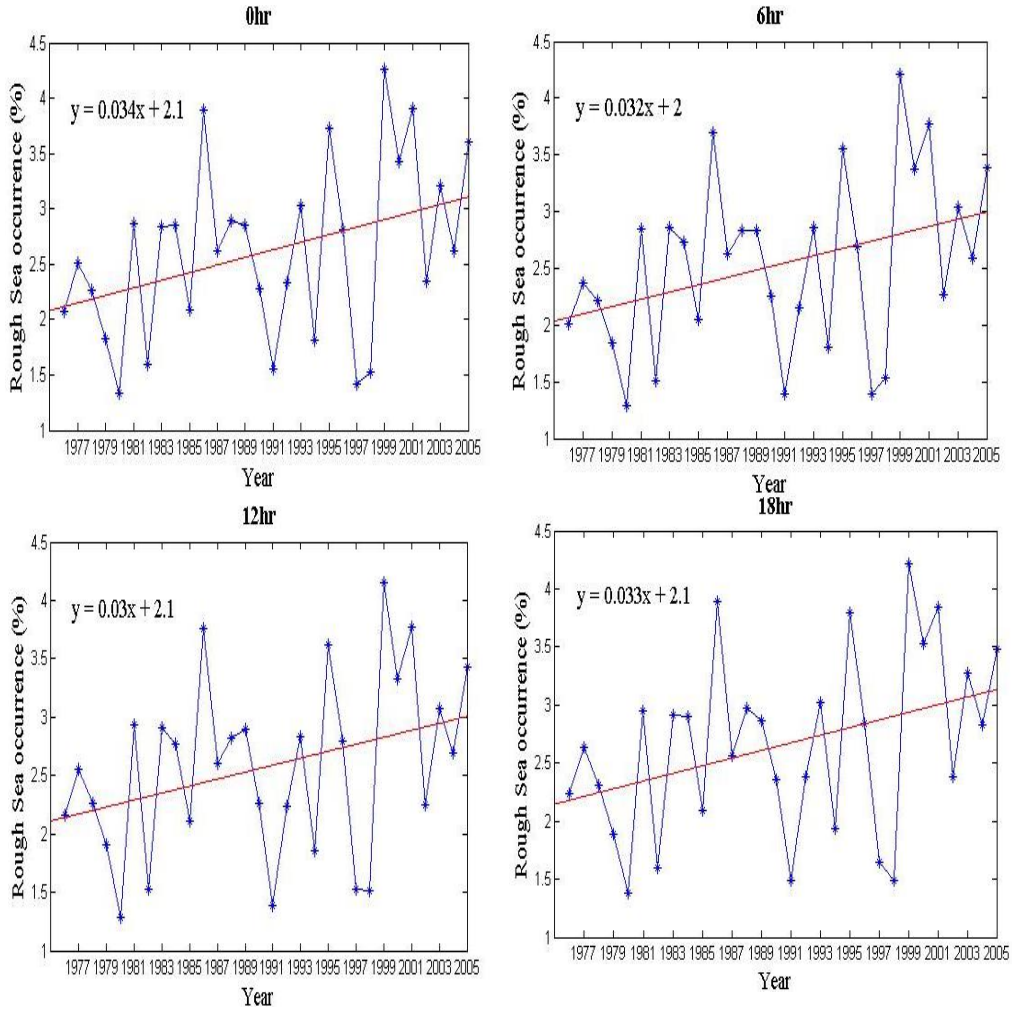

Figure 14. Linear trends and variations of the diurnal mean rough sea occurrence (%yr^{-1}) in the SCS based on the wave hindcast information (1976 to 2005).

occurrence are strongest (0.1 to 0.14% yr^{-1}) particularly in the Luzon strait and adjacent waters in the northern SCS. The trends are generally insignificant and decreasing in the southern SCS and in some few waters in the extreme northern SCS.

Temporal Distribution of Long-Term Trends in Rough Sea Occurrence

The temporal distributions of the annual, seasonal, monthly and diurnal trends in the rough sea occurrence are as shown in Figures 11, 12, 13 and 14. By using the method of linear regression, results for which are significant at the 95% probability level, the regression coefficient displayed in Figure 11 is 0.032. This means the rough sea occurrence exhibits a significant increasing trend of 0.032% yr^{-1} in the SCS between years 1976 and 2005. On the average, highest values (3.7 to 4.2%) of the rough sea occurrence are found in years 1986, 1995, 1999 and 2001. Lowest values (1.3 to 1.6%) are seen in years 1980, 1982, 1991, 1997 and 1998. In Figure 12, the rough sea occurrence exhibits a significant increasing trend of 0.12% yr^{-1}during winter. It peaked at 10.5 and 10.6%, respectively in years 1995 and 1999. Years 1979, 1980, 1982, 1991 and 1992 have the smallest values (<3%) of occurrence. During spring, the rough sea occurrence has a non-significant (0.0072% yr^{-1}) increasing trend. Rough sea occurrence is highest in years 1986 and 2005 with values of 2.1 and 1.9%, respectively. Least values (<0.2%) are found in years 1979, 1981, 1983, 1987, 1992, 1993, 1995, 1998, 2000 and 2002.

The rough sea occurrence exhibits a significant increasing trend of 0.039% yr^{-1} in the summer. It peaked at 4% in year 1992 and has a least value of 0.15% in year 1998. In the autumn, the rough sea occurrence showed a decreasing trend of -0.038% yr^{-1}. Maximum values of rough sea occurrence (6.8, 5.7 and 6.2%) are found, respectively in years 1983, 1986 and 1988 while

values less than 2% are found in years 1980, 1982, 1987, 1991, 1997, 1998 and 2002. In general, the increasing trend of the rough sea occurrence is most significant (0.12% yr^{-1}) in the winter while autumn exhibits a decreasing trend of -0.038% yr^{-1}. As shown in Figure 13,

increasing trends in rough sea occurrence exist in January, February, March, July, August and December while negative trends are observed in April, May, June, September, October and November. The increasing trend is most significant (0.25%yr^{-1}) in December and with peak percentage frequencies of rough sea in years 1993 (19%), 1995 (18.5%) and 1999 (22%). The increasing trend is least significant (0.028%yr^{-1}) in March and with maximum percentage frequencies of rough sea in years 1986 (5.4%), and 2005 (5.5%). Rough sea occurrence exhibits equal trends (0.075%yr^{-1}) in February and August.

In February, largest values (11.5 and 13.8%) in percentage frequencies of rough sea are seen, respectively in years 1977 and 1996 while in August, a peak value of 7.8% is seen in year 2002. Decreasing trends in rough sea occurrence is most significant (-0.061%yr^{-1}) in October and least significant (-0.0016%yr^{-1}) in April. In October, maximum percentage frequencies of rough sea (8.5 and 8.3%) occurred, respectively in years 1978 and 1992 while in April, the maximum percentage frequency (1.78%) occurred in year 1991. In May, June and September, the percentage frequencies of rough sea peaked at 2.3, 5.5 and 3.9%, respectively in years 1989, 1985 and 1977. In January, largest percentage frequencies of rough sea (13.8 and 13.9%) are observed in years 1986 and 2000. In July, the frequencies peak at 3.8, 4.4 and 3.8%, respectively in years 1996, 2001 and 2002. Moreover in November, the frequencies peaked at 15 and 14%, respectively in years 1983 and 1988. Lastly, in Figure 14, the rough sea occurrence exhibits positive trends and with slight differences for all the hours considered. The trend is most significant (0.034%yr^{-1}) at 0 h and least significant (0.03%yr^{-1}) at 12hr. In all hours, largest percentage frequencies (3.9, 3.7, 4.2 and 3.8%) of the rough sea respectively occurred in years 1986, 1995, 1999 and 2001.

CONCLUSIONS

Rough sea occurrence in the SCS is relatively low, of below 17% in each season. The relative high occurrence happened in winter (up to 16%) followed by Autumn (up to 12%), followed by Summer (up to 4.5%) and least in Spring (up to 1.6%) in the whole 30 years. The high occurrence during the winter is as a result of the predominance of the Northeast trade wind caused by frequent and powerful cold air. Regions such as Luzon strait, Dongsha, Xisha and Zhongsha in the Northern and central SCS are noted with significant large values of the rough sea occurrence whereas locations around Hainan and some waters around Palawan and Kalimantan in the Southern SCS are noted with significant low values. High percentage of occurrence distributes over a large part of the SCS in November, December and January and with largest values occurring in December.

The rough sea occurrence does not show much diurnal variation in the SCS. For the hours considered, the percentage frequency of the rough sea is largest around Luzon strait, Dongsha, Xisha and Zhongsha which are in the northern and central SCS. Considering the regional distribution of the annual trends of the rough sea occurrence, positive trends dominate most part of the SCS.

The relative large region distribute in the central and northern area of SCS. Increasing trends are most significant (0.1 to 0.13% yr^{-1}) around Luzon strait and adjacent waters. Long-term trend in the rough sea occurrence in the SCS also showed great seasonal differences. The areal extent of the significant increase in rough sea occurrence is largest in winter and smallest in autumn. Positive trends prevailed in all seasons except autumn. The increasing trend is generally strongest in winter, followed by summer and spring and weakest in autumn.

The rough sea occurrence exhibits significant increasing trends around Luzon strait, Dongsha and adjacent waters in the northern SCS during December, February, March and November. The trend in rough sea occurrence is strongest (up to 1% yr^{-1}) around Xisha in December. The trends in rough sea occurrence do not show much diurnal differences in the SCS. In all the hours considered, relatively large area of significant increasing trends (0.02 to 0.14% yr^{-1}) distribute in most waters of the central and northern SCS.

The trends in rough sea occurrence are strongest (0.1%-0.14% yr^{-1}) particularly in the Luzon strait and adjacent waters in the northern SCS. The rough sea occurrence exhibits a significant increasing trend of 0.032%yr^{-1} as a whole over a 30 year period in the SCS. The trend (0.12%yr^{-1}) is strongest in winter and weakest (-0.038%yr^{-1}) in autumn.

The increasing trend is most significant (0.25%yr^{-1}) in December and with peak percentage frequencies of rough sea in years 1993 (19%), 1995 (18.5%) and 1999 (22%). Lastly, the trend in rough sea occurrence is most significant (0.034%yr^{-1}) at 0 h. largest percentage frequencies (3.9, 3.7, 4.2 and 3.8%) of the rough sea respectively occurred in years 1986, 1995, 1999 and 2001.

Areas around Hainan, Kalimantan and Palawan with general low values of the rough sea occurrence are associated with shadowing, island blocking, refraction or complex topography. This study provides an overview of the rough sea climate which can be used for wave energy resource and as well as coastal zone management around the SCS.

ACKNOWLEDGEMENTS

This work is financially supported by the National Natural Science Foundation of China (51479183, 51509226), and the fundamental research funds for the central universities (201513040).

REFERENCES

Ahmed AU, 2010. Increased SST and Frequent Occurrence of Rough Sea Events in the Bay of Bengal: Implications for livelihoods of Coastal Populace in Bangladesh American Geophysical Union, Fall Meeting. abstract #GC32B-03.

Callahan PS, Morris CS, Hsiao SV (1994). Comparison of TOPEX/POSEIDON and significant wave height distributions to Geosat. J. Geophys. Res. 99:25015-25024.

Chu PC, Cheng KF (2008). South China Sea wave characteristics during Typhoon Muifa passage in winter 2004. J. Oceanogr. 64 (1): 1-21.

Chu PC, Lu SH, Liu WT (1999a). Uncertainty of the South China Sea prediction using NSCAT and NCEP winds during tropical storm Ernie 1996. J. Geophys. Res.104:273-11 289.

Dobson E, Monaldo F, Goldhirsh J (1987). Validation of Geosat altimeter-derived wind speeds and significant wave heights using buoy data, J. Geophys. Res. 92:10719-10731.

Edmons NL, Fan CW (1999b). Dynamical mechanisms for the South China Sea seasonal circulation and thermohaline variabilities. J. Phys. Oceanogr. 29:2971-2989.

Fu LL, Christensen EJ, Yamaone Jr CA, Lefebvre M, Menard Y, Dorrer M, Escudier P (1994). TOPEX/POSEIDON mission overview. J. Geophys. Res. 99: 24369-24381.

Moon IJ (2005). Impact of a coupled ocean wave-tide circulation system on coastal modeling. Ocean Model. 8: 203-236.

Schneggenburger C, Gunther H, Rosenthal W (2000). Spectral wave modeling with non-linear dissipation: Validation and applications in a coastal tidal environment. Coast. Eng. 41: 201-235.

Sundar V, Ananth PN (1988). Wind climate for Madras harbor, India. J. Wind Eng. Ind. Aerodynam., 31: 323-333.

Tolman HL,2009. User Manual and System Documentation of WAVEWATCH-III Version 3.14. NOAA/NWS/NCEP/MMAB Technical Note, Washington, 1-194.

Veneziano JM, Fan CW (2000). Response of the South China Sea to tropical cyclone Ernie 1996. J. Geophys. Res. 105:13991-14009.

Wang Z, Liangming Z, Sheng D, Lunyu W, Zhanbin L, Lin M, Aifang W (2014). Wind Wave Characteristics and Engineering Environment of the South China Sea. J. Ocean Univ. China (Oceanic and Coastal Sea Research) 13 (6): 893-900. DOI 10.1007/s11802-014-2331-0

Zheng CW, Zhou L, Huang CF, Shi YL, Li JX, Li J (2013a). The long-term trend of a sea surface wind speed and a (wind wave, swell, mixed wave) wave height in global ocean during the last 44 a, Acta Oceanol. Sin. 32(10): 1-4.

Zheng CW, Zhou L, Jia BK, Pan J, Li X (2014). Wave characteristic analysis and wave energy resource evaluation in the China Sea. J.Renew. Sustain. Energy 6.043101, doi: 10.1063/1.4885842.